Tests of maximum entropy reconstruction on simulated HESSI data

Benjamin A.C. Eves

1 Introduction

Maximum Entropy Methods (MEMs) provide an excellent method of image reconstruction for limited data such as the HESSI modulation profiles,the data is limited in the sense that some of the information from the object is missing due to the grids used to obtain the profile. The question remains as to how representative these reconstructions are of the original flare, as very different images can be obtained from the same modulation profile. To this end I have run numerous reconstructions of three test cases, for both MEM_SATO and MEM_VIS, to assess the effect the initial entropy multiplier has on reconstructions of sources with various brightness and compactness.

2 Method

The initial entropy multiplier `lnorm` governs the initial weighting for the entropy. For small values, entropy is a strong constraint to the detriment of a good χ^2. Conversely, for large `lnorm` values entropy is a weaker constraint and leads to a good fit to data, $\chi^2 = 1$, but can lead to the breaking up of smooth, extended sources. Due to this we attempted to find the best values for `lnorm` in both MEM_SATO and MEM_VIS for three different types of source at varying brightnesses, in order to reconstruct the most realistic image. The three test sources are a point source, a 10"x 20" gaussian and a 20"x40"gaussian of the same total brightness. The simulations were generated through the hsi_image object, defining three gaussians,one with `xysigma` set to default (0.001, 0.001),one of `xysigma`=[10.,20.], and one of `xysigma`=[20.,40.]. To make the test equal for both algorithms CHI_LIMIT was set to MEM_SATO's default of 1.03 for both and LAMBDA_MAX to 150. Thus the reconstructions end if LAMBDA reaches 150 or if a χ^2 of 1.03 is reached, MEM_SATO also stops if χ^2 is not decreasing fast enough or if it reaches the maximum number of iterations for a given LAMBDA.

With these constraints we then ran image reconstructions of all three sources for the following `lnorm` and SIM_PHOTONS_PER_COLL (number of photons per collimator per second).

SIM_PHOTONS_PER_COLL = 7500, 37500, 75000, 375000.

MEM_SATO `lnorm` = 1, 0.5, 0.1, 5e-2, 1e-2.

MEM_VIS `lnorm` = 1e-3, 5e-3, 1e-4, 5e-5, 1e-5.

NB. The default `lnorm` for MEM_SATO is 0.1 and for MEM_VIS 1e-5.

After each reconstruction the reconstructed image was saved along with the parameters `btot`, final χ^2, number of lambda iterations. The parameter `btot` is the total image brightness used in the reconstruction algorithm. Since the energy range is set to 6kev to 100kev `btot` should be somewhat less than the value of SIM_PHOTONS_PER_COLL as we lose a lot of photons at the lower energies.

3 Results

Both algorithms could reconstruct the point source with little difficulty so we only present the reconstructed images of the extended sources for certain arbitrary input parameters. Each image has its associated `lnorm` and SIM_PHOTONS-_PER_COLL value printed below it. All figures are 64 x 64 images with 4" x 4" pixels.

Figures 1 and 3 show that changes to SATO_LNORM has little effect over our range and MEM_SATO has difficulty in identifying that the source is a single large source rather than a collection of points. MEM_SATO performs better at higher counts and for the 10" x 20" source at 375000 photons we see a definite single extended source with little spurious structure. For the 20" x 40" source at high counts we see the extended source as a cluster of point sources plus some faint tendril like structure, at low counts the central source is indistinguishable from the background of spurious point sources.

Figures 2 and 4 show that with a small `lnorm` MEM_VIS reconstructs a diffuse source but shows much structure where there is none. For higher `lnorm` the image resembles a collection of point sources, this is true for both extended sources, although the 10" x 20" source shows less internal structure than the 20" x 40" source. At high counts even at `lnorm`=1e-4 we see a collection of point sources for both test simulations.

For MEM_SATO, at high counts the image is relatively less fragmented at the same `lnorm` than for lower counts. For MEM_VIS the opposite is as less internal structure is present for increasing counts for `lnorm`=1e-5.

The fragmentation could be caused by the systematic errors that MEM_ VIS includes, as they become more important at higher counts therefore a χ^2 of 1 is a fit to the systematic errors rather than a fit to the relevant data. This is due to the way the standard deviation for the data is calculated in MEM_VIS as this includes the systematic errors which scale approximately as the square of the counts and so at high counts these systematic errors dominate the data.

Another cause of spurious structure could be the fact that both MEM_SATO and MEM_VIS use the modulations from all detectors given as default (i.e. 4, 5, 6, 7, and 8 of the 9 detectors) ,where 1 is the finest and 9 is the coarsest detector, even if they contain no relevant modulation. This give spurious structure since for a large extended source the modulation of the fine grids would be negligible.

To test this hypothesis a further reconstruction run was performed using only detectors 6, 7, and 8. For SATO_LNORM 0.1, and 1e-2, VIS_LNORM 1e-4, and 1e-5.

3.1 Results: Reconstructions with only detectors 5, 6, and 7.

We can see from figure 5 that although MEM_SATO still produces images with spurious structure at the lower counts there is no breaking up of the image in to point sources and there is a definite large central source. At the higher counts we get a good representation of the 20" x 40" source. The same can be said for the 10" x 20" source in figure 7, although at the lower counts we do see less spurious structure than for the more diffuse larger source.

MEM_VIS (figure 6) also shows less internal structure than previously but still displays fragmentation at high counts, and for `lnorm`=1e-5, SIM_PHOTONS-_PER_COLL = 375000 the image is even more fragmented than the default detectors run. A similar occurrence can be seen in figure 8 for the 10"x 20" source. Note that the final run in figure 8 was performed with a different realisation of the simulated model, to the others due to software problems, this is also why the final `btot` is relatively lower than the other SIM_PHOTONS_PER_COLL = 375000 run compared to the lower count runs.

4 Conclusions

Both MEM_VIS and MEM_SATO performed well on the point sources, with little change between `lnorm`'s. For low counts MEM_VIS performs much better than MEM_SATO for the 20" x 40" gaussian source, but for the 10" x 20" it returns a more accurately reconstructed image for only the lowest counts and MEM_SATO produces more consistent reconstructions for increasing counts. We must bear in mind that, unlike MEM_VIS, MEM_SATO does not have any systematic errors and so at high counts where they would dominate we see no evidence of this and so see no image break up in figure 7 at high counts.

In terms of the increasing of the initial entropy multiplier `lnorm` we see very little effect on the MEM_SATO reconstructions over the range 1 to 1e-2 and it would appear that counts are the dominant factor. In MEM_VIS high counts cause image break up due to fitting of the systematic errors, but for low to medium counts (7500 to 75000) the effect of increasing the value of `lnorm` from it's default of 1e-5 is extremely noticeable and causes a great deal of fragmentation.

MEM_SATO is robust to the point of being ignorant to changes in `lnorm`, but this could be due to the entropy constraint being effectively turned off at `lnorm` ≥ 0.1 and so increasing `lnorm` is effectively useless. MEM_SATO also performed better for the smaller sources than the large diffuse source and this is worth bearing in mind for future work. It would be interesting to see if image fragmentation increased with increasing counts if the systematic errors were present in the simulation.

MEM_VIS is very sensitive to increases in `lnorm`, but at it's default (1e-5) performs well for counts < 375000 in this test, before systematic errors dominate. It outperforms MEM_SATO for the 20" x 40" source in both detector regimes apart from at higher counts.

In conclusion, MEM_SATO as it is now is very good for smaller sources at high counts, MEM_VIS is better at low `lnorm` and low counts, and for larger diffuse sources.

Table 1: MEM_SATO output for 20"x40" gaussian source

Source	Photons/s^{-1} /coll.	`lnorm`	Final χ^2	No. of Lambda iterations	`btot`
20"x40"	7500	1	1.02954	1	919.865
20"x40"	7500	0.5	1.02918	2	922.201
20"x40"	7500	0.1	1.02914	10	922.219
20"x40"	7500	5e-2	1.02917	20	922.131
20"x40"	7500	1e-2	1.02863	101	921.907
20"x40"	37500	1	0.997760	2	4530.33
20"x40"	37500	0.5	0.997128	4	4532.76
20"x40"	37500	0.1	1.01764	17	4535.49
20"x40"	37500	5e-2	1.02642	32	4536.34
20"x40"	37500	1e-2	1.04281	144	4537.86
20"x40"	75000	1	1.02463	3	8984.23
20"x40"	75000	0.5	1.02485	6	8988.52
20"x40"	75000	0.1	1.02737	29	8989.87
20"x40"	75000	5e-2	1.02548	59	8989.33
20"x40"	75000	1e-2	1.13944	144	9010.25
20"x40"	375000	1	1.41799	2	44246.9
20"x40"	375000	0.5	1.01564	6	44131.3
20"x40"	375000	0.1	1.02367	29	44189.2
20"x40"	375000	5e-2	1.02086	59	44188.3
20"x40"	375000	1e-2	1.23208	144	44271.2

Table 2: MEM_VIS output for 20"x40" gaussian source

Source	Photons/s^{-1} /coll.	`lnorm`	Final χ^2	No. of Lambda iterations	`btot`
20"x40"	7500	1e-3	0.989943	1	893.670
20"x40"	7500	5e-3	1.02055	4	893.670
20"x40"	7500	1e-4	1.02993	4	893.670
20"x40"	7500	5e-5	1.00702	7	893.670
20"x40"	7500	1e-5	1.02828	32	893.670
20"x40"	37500	1e-3	1.02279	30	4578.24
20"x40"	37500	5e-3	1.02260	46	4578.24
20"x40"	37500	1e-4	0.987434	5	4578.24
20"x40"	37500	5e-4	1.02347	8	4578.24
20"x40"	37500	5e-5	1.01984	40	4578.24
20"x40"	75000	1e-3	1.01462	117	9190.06
20"x40"	75000	5e-3	1.05965	157	9190.06
20"x40"	75000	1e-4	1.02485	49	9190.06
20"x40"	75000	5e-5	0.994111	11	9190.05
20"x40"	75000	1e-5	1.02846	46	9190.05
20"x40"	375000	1e-3	2.43638	156	45055.6
20"x40"	375000	5e-3	1.65805	163	45055.6
20"x40"	375000	1e-4	1.96414	160	45055.6
20"x40"	375000	5e-5	2.18794	164	45055.7
20"x40"	375000	1e-5	0.928651	56	45055.6

(a) 0.1,7500 (b) 1e-2,7500

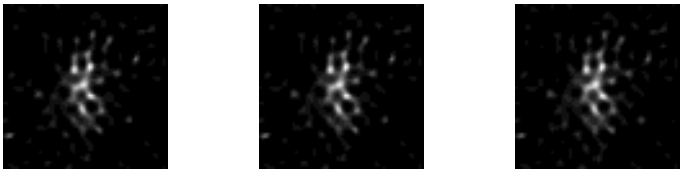

(c) 1,37500 (d) 0.5,37500 (e) 0.1,37500

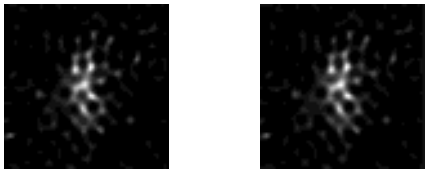

(f) 5e-2,37500 (g) 1e-2,37500

(h) 0.1,75000 (i) 1e-2,75000

(j) 0.1,375000 (k) 1e-2,375000

Figure 1: Reconstructed images for a 20"by 40" Gaussian Source with MEM_SATO

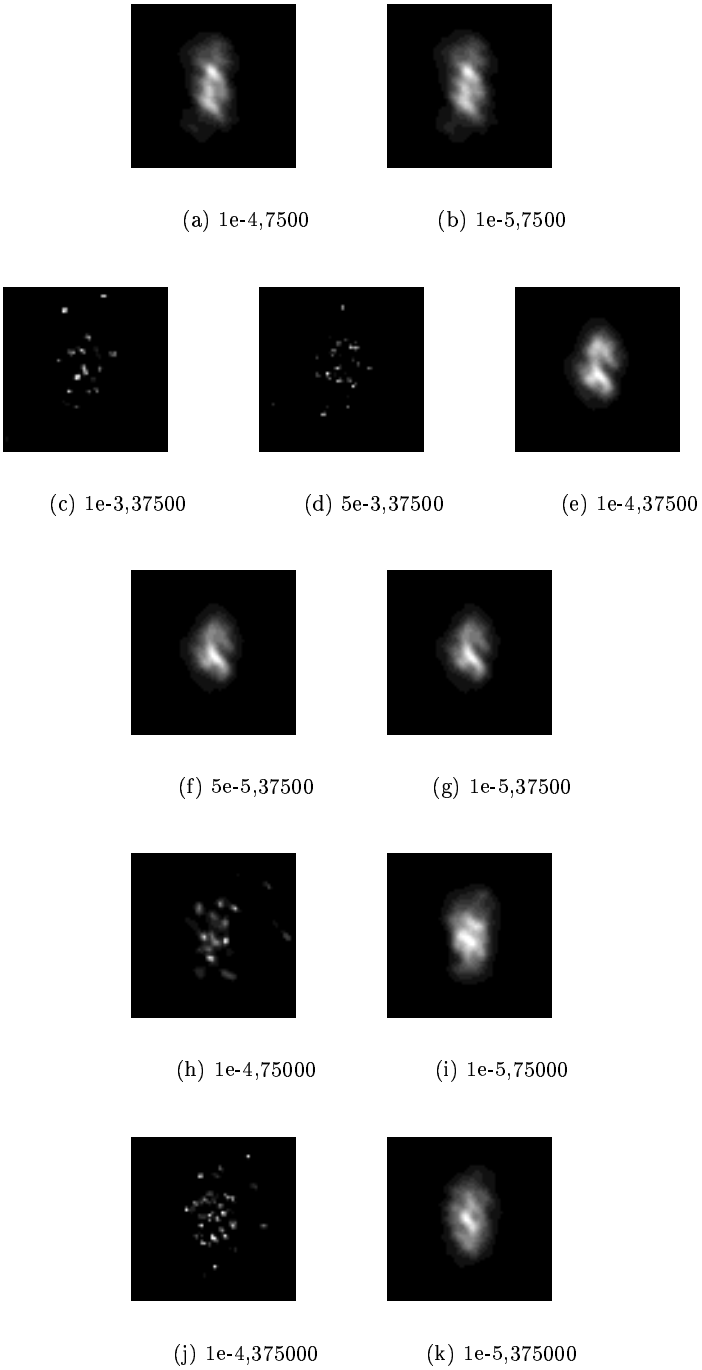

(a) 1e-4,7500 (b) 1e-5,7500

(c) 1e-3,37500 (d) 5e-3,37500 (e) 1e-4,37500

(f) 5e-5,37500 (g) 1e-5,37500

(h) 1e-4,75000 (i) 1e-5,75000

(j) 1e-4,375000 (k) 1e-5,375000

Figure 2: Reconstructed images for a 20" by 40" Gaussian Source with MEM_VIS

Table 3: MEM_SATO output for 10"x20" gaussian source

Source	Photons/s^{-1} /coll.	`lnorm`	Final χ^2	No. of Lambda iterations	`btot`
10"x20"	7500	1	1.02802	4	915.771
10"x20"	7500	0.5	1.02800	8	915.868
10"x20"	7500	0.1	1.02870	39	915.774
10"x20"	7500	5e-2	1.19378	17	928.977
10"x20"	7500	1e-2	1.09863	144	922.768
10"x20"	37500	1	1.02566	3	4492.88
10"x20"	37500	0.5	1.02635	6	4496.92
10"x20"	37500	0.1	1.02863	29	4498.47
10"x20"	37500	5e-2	1.02664	59	4497.88
10"x20"	37500	1e-2	1.15432	144	4516.25
10"x20"	75000	1	1.00566	3	8996.56
10"x20"	75000	0.5	1.00820	6	9009.82
10"x20"	75000	0.1	1.02729	26	9022.18
10"x20"	75000	5e-2	1.01824	55	9019.43
10"x20"	75000	1e-2	1.17556	144	9054.24
10"x20"	375000	1	1.78405	2	43436.3
10"x20"	375000	0.5	1.19679	6	44077.3
10"x20"	375000	0.1	1.02972	43	44092.6
10"x20"	375000	5e-2	1.02812	86	44100.8
10"x20"	375000	1e-2	1.39365	144	44252.2

Table 4: MEM_VIS output for 10"x20" gaussian source

Source	Photons/s^{-1} /coll.	`lnorm`	Final χ^2	No. of Lambda iterations	`btot`
10"x20"	7500	1e-3	1.02161	1	903.703
10"x20"	7500	5e-3	1.00142	2	903.703
10"x20"	7500	1e-4	1.02759	4	903.703
10"x20"	7500	5e-5	1.02755	8	903.703
10"x20"	7500	1e-5	1.02605	41	903.703
10"x20"	37500	1e-3	0.873270	14	4633.52
10"x20"	37500	5e-3	0.978479	8	4633.52
10"x20"	37500	1e-4	0.939075	4	4633.52
10"x20"	37500	5e-5	1.00918	7	4633.52
10"x20"	37500	1e-5	1.01349	35	4633.52
10"x20"	75000	1e-3	1.02265	56	9318.74
10"x20"	75000	5e-3	1.02444	38	9318.74
10"x20"	75000	1e-4	0.961857	11	9318.74
10"x20"	75000	5e-5	0.986234	16	9318.74
10"x20"	75000	1e-5	1.02419	60	9318.75
10"x20"	375000	1e-3	2.12918	158	45453.8
10"x20"	375000	5e-4	2.20359	162	45453.8
10"x20"	375000	1e-4	2.85454	156	45453.8
10"x20"	375000	5e-5	2.16552	155	45453.8
10"x20"	375000	1e-5	1.34413	160	45453.8

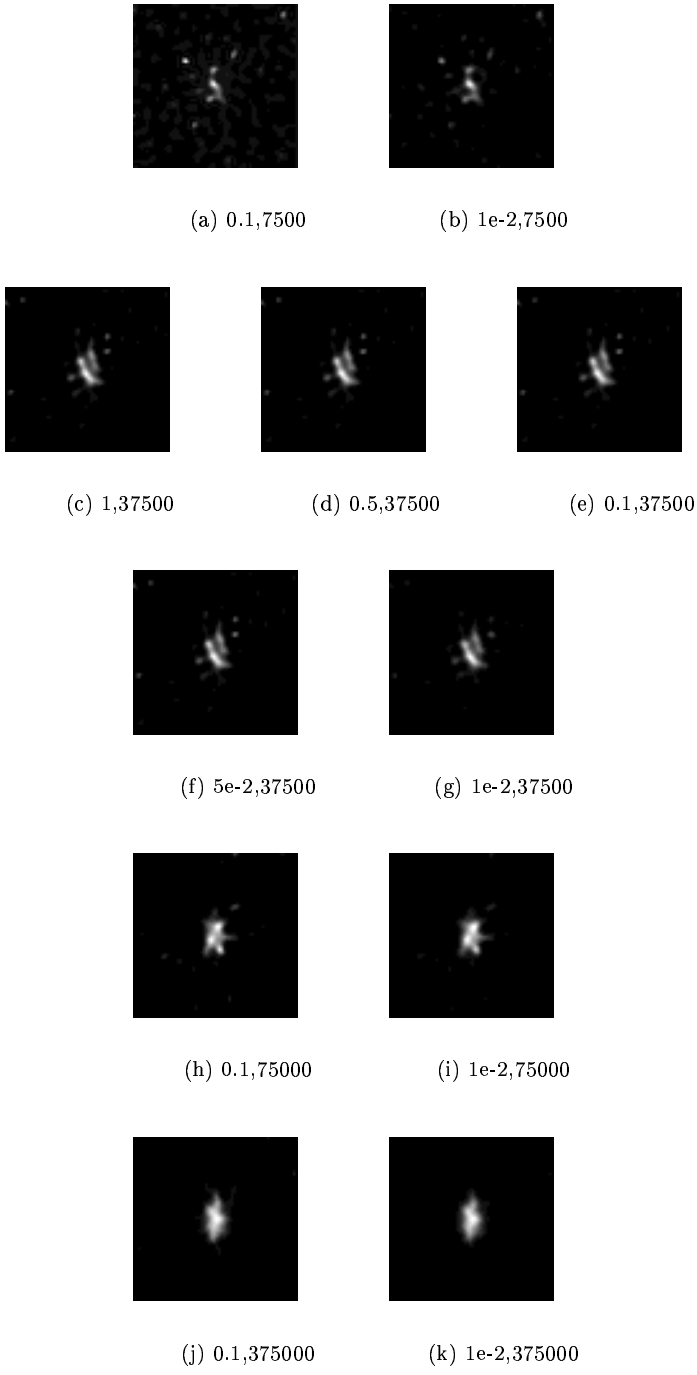

(a) 0.1,7500 (b) 1e-2,7500

(c) 1,37500 (d) 0.5,37500 (e) 0.1,37500

(f) 5e-2,37500 (g) 1e-2,37500

(h) 0.1,75000 (i) 1e-2,75000

(j) 0.1,375000 (k) 1e-2,375000

Figure 3: Reconstructed images for a 10" by 20" Gaussian Source with MEM_SATO

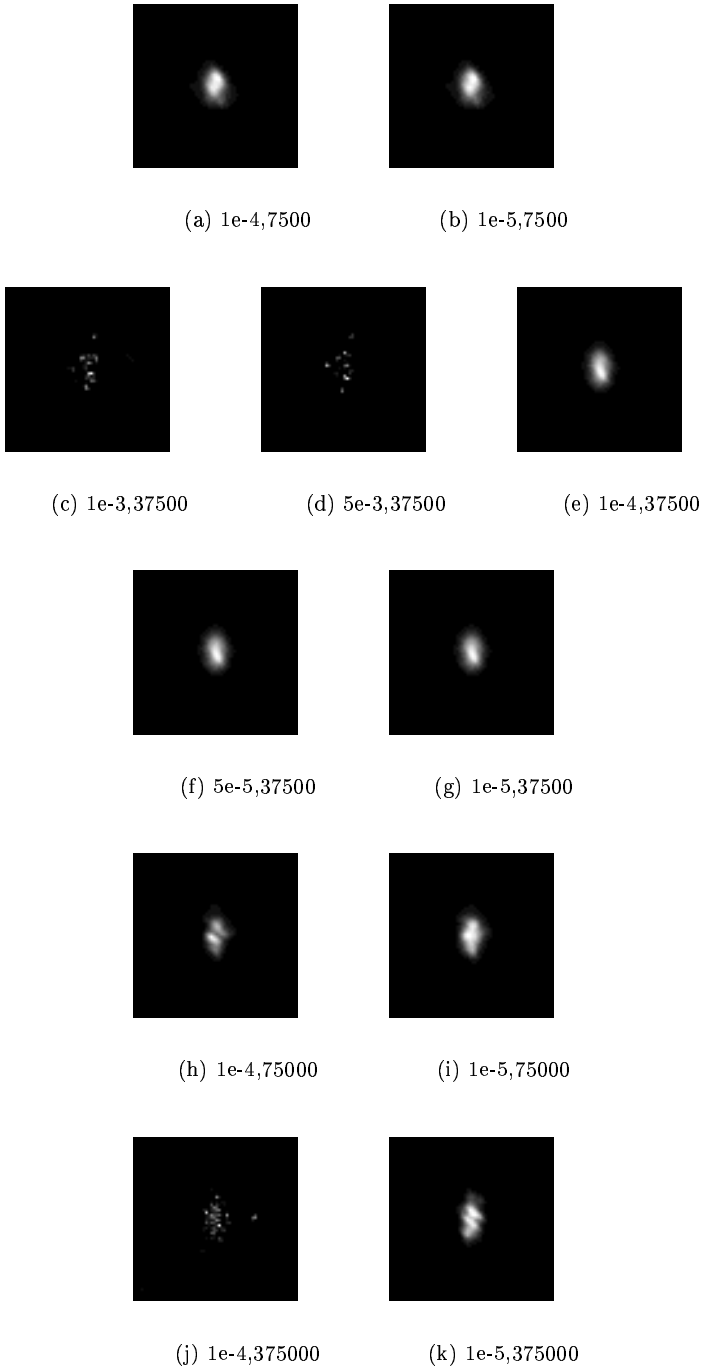

(a) 1e-4,7500 (b) 1e-5,7500

(c) 1e-3,37500 (d) 5e-3,37500 (e) 1e-4,37500

(f) 5e-5,37500 (g) 1e-5,37500

(h) 1e-4,75000 (i) 1e-5,75000

(j) 1e-4,375000 (k) 1e-5,375000

Figure 4: Reconstructed images for a 10" by 20" Gaussian Source with MEM_VIS

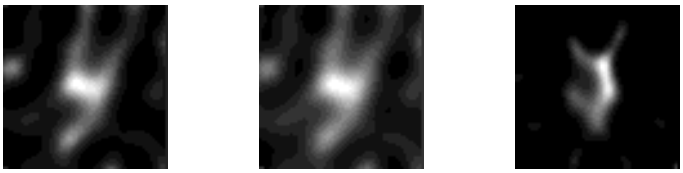

(a) 0.1,7500 (b) 1e-2,7500 (c) 0.1,37500

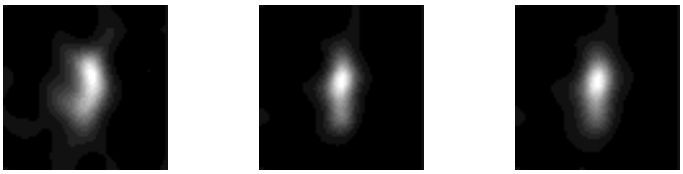

(d) 1e-2,37500 (e) 0.1,75000 (f) 1e-2,75000

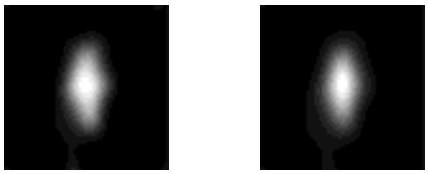

(g) 0.1,375000 (h) 1e-2,375000

Figure 5: MEM_SATO reconstructions for a 20" by 40" Gaussian source using detectors 5, 6 and 7

Table 5: MEM_SATO output for 20"x 40" gaussian source using detectors 5, 6 and 7.

Source	Photons/s^{-1} /coll.	`lnorm`	Final χ^2	No. of Lambda iterations	`btot`
20"x40"	7500	0.1	1.01823	29	917.476
20"x40"	7500	1e-2	1.11463	144	922.853
20"x40"	37500	0.1	1.05591	144	4524.14
20"x40"	37500	1e-2	1.64439	144	4565.35
20"x40"	75000	0.1	1.02719	39	8987.78
20"x40"	75000	1e-2	1.55925	144	9039.77
20"x40"	375000	0.1	1.02024	59	44001.2
20"x40"	375000	1e-2	2.24007	144	44257.1

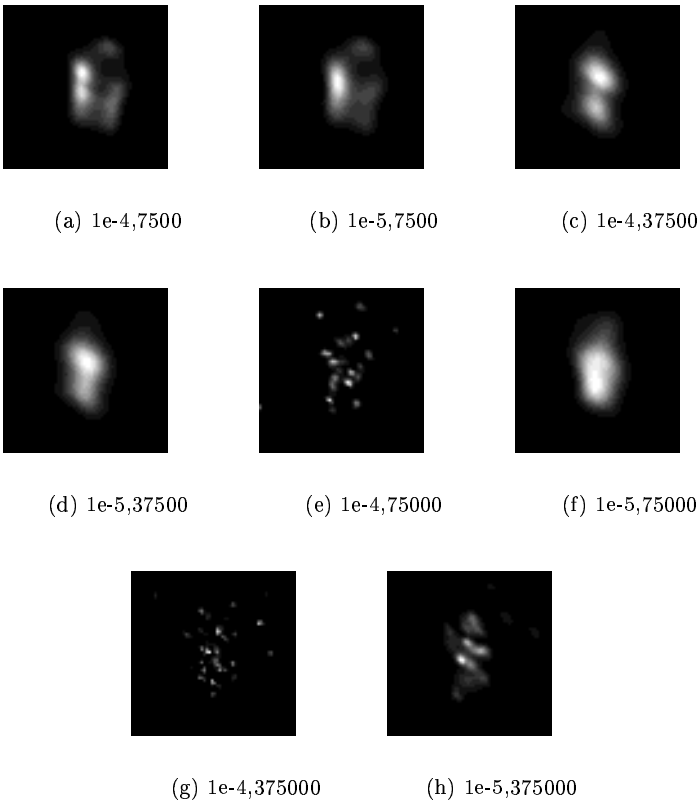

(a) 1e-4,7500 (b) 1e-5,7500 (c) 1e-4,37500

(d) 1e-5,37500 (e) 1e-4,75000 (f) 1e-5,75000

(g) 1e-4,375000 (h) 1e-5,375000

Figure 6: MEM_VIS reconstructions for a 20" by 40" Gaussian source using detectors 5, 6 and 7

Table 6: MEM_VIS output for 20"x 40" gaussian source using detectors 5, 6 and 7.

Source	Photons/s^{-1} /coll.	`lnorm`	Final χ^2	No. of Lambda iterations	`btot`
20"x40"	7500	1e-4	1.01975	14	918.490
20"x40"	7500	1e-5	1.02770	86	918.490
20"x40"	37500	1e-4	0.946660	2	4641.58
20"x40"	37500	1e-5	1.01895	24	4641.58
20"x40"	75000	1e-4	0.991678	103	9281.58
20"x40"	75000	1e-5	1.02819	39	9281.58
20"x40"	375000	1e-4	2.25146	154	46022.8
20"x40"	375000	1e-5	1.80311	159	46022.8

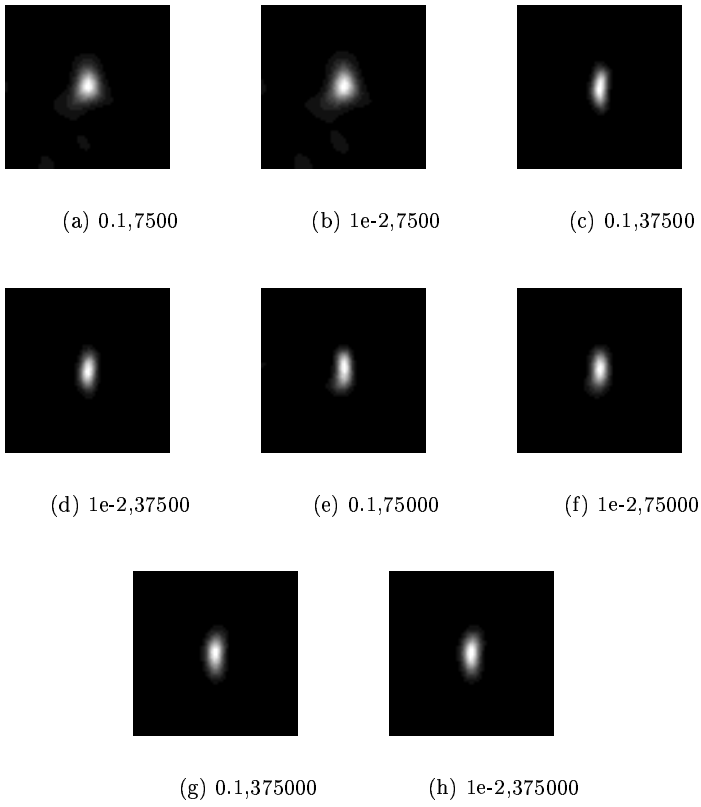

(a) 0.1,7500 (b) 1e-2,7500 (c) 0.1,37500

(d) 1e-2,37500 (e) 0.1,75000 (f) 1e-2,75000

(g) 0.1,375000 (h) 1e-2,375000

Figure 7: MEM_SATO reconstructions for a 10" by 20" Gaussian source using detectors 5, 6 and 7

Table 7: MEM_SATO output for 10"x 20" gaussian source using detectors 5, 6 and 7.

Source	Photons/s^{-1} /coll.	`lnorm`	Final χ^2	No. of Lambda iterations	`btot`
10"x20"	375000	0.1	1.00119	6	911.155
10"x20"	375000	1e-2	1.02026	51	911.861
10"x20"	375000	0.1	1.02879	32	4572.84
10"x20"	375000	1e-2	1.06240	144	4594.27
10"x20"	375000	0.1	1.05007	47	8963.04
10"x20"	375000	1e-2	1.09474	144	9025.45
10"x20"	375000	0.1	1.05695	17	43800.0
10"x20"	375000	1e-2	1.05980	144	43938.9

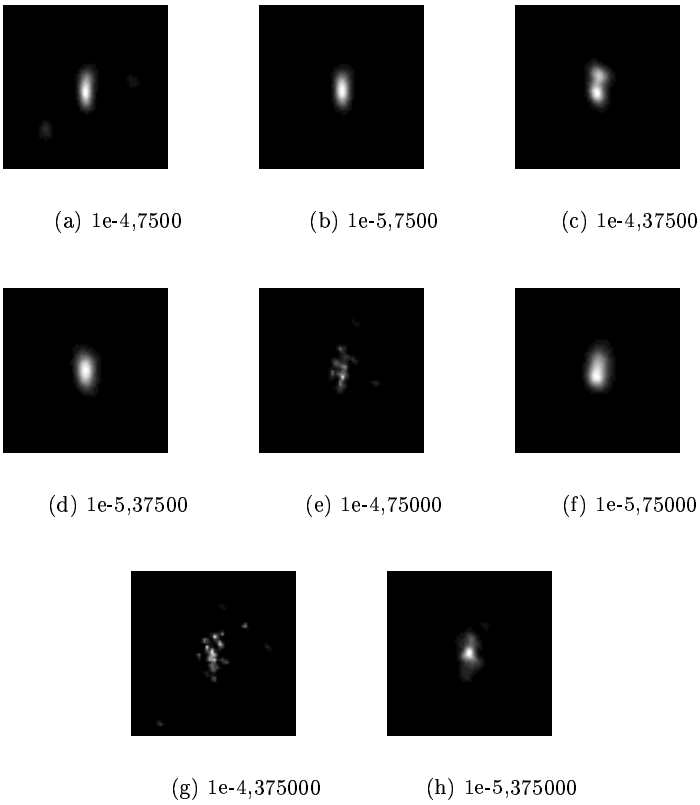

(a) 1e-4,7500 (b) 1e-5,7500 (c) 1e-4,37500

(d) 1e-5,37500 (e) 1e-4,75000 (f) 1e-5,75000

(g) 1e-4,375000 (h) 1e-5,375000

Figure 8: MEM_VIS reconstructions for a 10" by 20" Gaussian source using detectors 5, 6 and 7

Table 8: MEM_VIS output for 10"x 20" gaussian source using detectors 5, 6 and 7.

Source	Photons/s^{-1} /coll.	`lnorm`	Final χ^2	No. of Lambda iterations	`btot`
10"x20"	7500	1e-4	1.00633	16	938.392
10"x20"	7500	1e-5	1.02658	89	938.393
10"x20"	37500	1e-4	0.941917	5	4786.80
10"x20"	37500	1e-5	1.02470	39	4786.80
10"x20"	75000	1e-4	0.974852	93	9567.29
10"x20"	75000	1e-5	1.01323	57	9567.30
10"x20"	375000	1e-4	3.58245	157	46874.7
10"x20"	375000	1e-5	2.17352	159	46923.4